Journal of Information Security and Applications 000 (2017) 1–10

Contents lists available at ScienceDirect

Journal of Information Security and Applications

journal homepage: www.elsevier.com/locate/jisa

Detection of image seam carving by using weber local descriptor and local binary patterns

Dengyong Zhang[a,b], Qingguo Li[c], Gaobo Yang[a,*], Leida Li[d], Xingming Sun[e]

[a] School of Information Science and Engineering, Hunan University, Changsha 410082, China
[b] School of Computer & Communication Engineering, Changsha University of Science & Technology, Changsha 410005, China
[c] College of Mathematics and Economics, Hunan University, Changsha 410082, China
[d] School of Information and Electrical Engineering, China University of Mining and Technology, Xuzhou 221116, China
[e] School of Computer and Software, Nanjing University of Information Science & Technology, Nanjing 210044, China

ARTICLE INFO

Article history:
Available online xxx

Keywords:
Image forensics
Weber local descriptor (WLD)
Local binary patterns (LBP)
Kruskal–Wallis statistic
Seam carving

ABSTRACT

Seam carving is a popular content-aware image resizing technique by removing unnoticeable seams with low energies for aesthetic purpose. However, it might also be used for malicious forgeries such as object removal. In this paper, a blind forensics approach is proposed to detect resized images by seam carving. Since seam carving mainly changes local textures, two excellent texture descriptors including Weber Local Descriptor (WLD) and Local Binary Patterns (LBP) are exploited for seam carving forgery detection. Specifically, the histogram features of WLD and LBP are extracted from candidate images, respectively. Then, Kruskal–Wallis statistic is exploited to select a subset of more discriminative features. Finally, support vector machine (SVM) is exploited as classifier to judge whether an image is original or suffered from seam carving. Extensive experiment results on a large set of test images show that the proposed approach achieves better performance than the state-of-the-art approaches.

1. Introduction

With the popularity of inexpensive and portable image capture devices such as mobile phone, almost everybody can conveniently record and share digital images nowadays. Meanwhile, it is increasingly easier for ordinary users to create tampered images with various image editing software such as PhotoShop. Moreover, the tampered images are very difficult, if not impossible, to be distinguished from authentic photographs by naked eyes. Thus, image forgery detection is an active topic in the field of information security [1]. Seam carving is a widely-accepted content-aware image resizing technique for aesthetic purpose. It achieves superior resizing performance by compromising well between protecting important region and keeping overall content. Seam carving has been adopted in PhotoShop CS 6 and GIMP as adaptive scaling [2]. However, seam carving can also be used for malicious purposes. Firstly, it might be used to correct photo composition, which will be a cheating when the resultant image is used for photo competition. Secondly, it can also be deliberately used for object removal, which usually changes image semantics. Therefore, it is worthy of investigation to design a detection approach to expose those retargeted images after seam carving.

In recent years, there exist several approaches for seam carving forgery detection. Lu et al. presented an active approach to detect seam carving by exploiting the well-designed side information called forensic hash [3]. It is effective for seam carving detection and can even estimate some key parameters. However, forensic hash is usually forgery-specific and should be built in advance. Moreover, it might be removed by falsifiers. For blind detection, Sarkar et al. made the first attempt by exploiting 324D Markov features from candidate images to unveil seam carving [4]. Later, Fillion et al. proposed a detection approach by exploiting a set of intuitively motivated features such as wavelet absolute moments. For the resized images with more than 30% shrinkage, it improves the detection accuracy up to 91% [5]. Wei et al. presented a patch analysis approach for seam carving detection [6]. Suspicious images are divided into mini-squares. Then, an optimal type of patch is searched from nine types for each mini-square, which is likely to recover a mini-square from seam carving. Finally, Markov features are constructed by considering patch transition probabilities for connecting mini-squares in the subdiagonal, vertical and diagonal directions. It achieves detection accuracies up to 92.2%, 92.6% and 95.8% for resized images with 20%, 30% and 50% shrinkages, respectively. Motivated by the changes of energy and noise distri-

* Corresponding author.
E-mail address: yanggaobo@hnu.edu.cn (G. Yang).

http://dx.doi.org/10.1016/j.jisa.2017.09.003
2214-2126/

bution, Ryu et al. presented an energy bias and noise based approach for seam carving detection [7]. In our recent work, local binary pattern (LBP) is introduced into seam carving detection [8]. It exploits the same features of energy and noise bias, which are extracted in LBP domain instead of pixel-domain. Since LBP highlights the texture changes caused by seam carving, it leads to better performances over the state-of-the-art approaches.

We still believe that if the inherent mechanism of seam carving are fully considered and the visual distortions caused by seam carving are further exploited, more discriminative features specific to seam carving forgery are possible to be designed to improve detection accuracy. The content-aware mechanism of seam carving makes the resized images without any common and noticeable distortions such as blurriness in blind forensics. Instead, information loss and possible shape distortions such as geometric deformation are the main artifacts of seam carving. However, it is still an open issue to measure geometric deformation and information loss without reference image in the field of image quality assessment (IQA). This is also a great challenge for seam carving detection. Thus, local and global texture changes are more feasible for seam carving detection than explicitly modeling shape distortions and information loss. In our earlier work [8], LBP, which is a simple yet effective local texture descriptor, is exploited to unveil local texture changes for seam carving detection. However, LBP considers only the signs of pixel differences between central pixel and its neighboring pixels. That is, LBP-based feature is an index of discrete patterns rather than a numerical feature, and can not provide any intensity information about image texture [9]. Luckily, weber local descriptor (WLD) is also an excellent texture descriptor for texture description and classification. It is composed of differential excitation and orientation [10]. Motivated by the fact that multiple texture descriptors might significantly improve texture classification performance compared with single descriptor, we attempt to simultaneously exploit LBP and WLD for feature extraction to improve the accuracy of seam carving forgery detection. Specifically, candidate images are firstly divided into blocks, and both LBP-based and WLD-based histogram features are extracted from each block. Then, Kruskal–Wallis statistic is exploited to select a subset of more discriminative features from them. Finally, SVM is exploited as classifier to judge whether an image has been suffered from seam carving or not.

The rest paper is organized as follows: Section 2.1 summaries image seam carving and makes a preliminary analysis of its detection. Section 3 briefly introduces LBP and WLD. Section 4 presents the proposed blind detection approach. Section 5 reports the experimental results and analysis, and we conclude this paper in Section 6.

2. Image seam carving and its possible artifacts for blind forensics

2.1. Preliminaries of seam carving

Seam carving is a content-aware image resizing technique. A seam is an 8-connected path of single pixel width, either from top to bottom or from left to right. Let I be an image of size $M \times N$. Let a vertical seam be an example. It is restricted by the horizontal offsets of no more than one pixel between adjacent rows. That is,

$$s^{v} = \{(i, col(i))\}_{i=1}^{n}, s.t. \forall i, |col(i) - col(i-1)| \leq 1 \quad (1)$$

where i and $col(i)$ are the row and column coordinates, respectively. A vertical seam s is defined by summing the energies of those pixels along a connected path from top to bottom. Please note that the optimal seam s^* is found by minimizing the energy via dynamic programming, as shown in Eq. (2). The energy value of single pixel is given by Eq. (3), which is a Sobel-operator-based function.

$$s^* = \min_{s}\{E(s)\} = \min_{s, s=\{s_i\}_{i=1}^{n}} \left\{ \sum_{i=1}^{n} e(I(s_i)) \right\} \quad (2)$$

$$e(I) = \left| \frac{\partial}{\partial x} I \right| + \left| \frac{\partial}{\partial y} I \right| \quad (3)$$

To remove a vertical seam, the most adjacent pixels, which are located at the right side of those pixels along this seam, are moved left one pixel to fit the gap left by seam removal. Since a seam is a connected path with minimum energy, removing such a seam has less impact on the resultant image. In most cases, image seam carving preserves well visually important content by successively removing unnoticeable seams. Fig. 1 is an example of image seam carving with 30% vertical shrinkage. Fig. 1(a) is the original image. From Figs. 1(b) and (c), we observe that seams firstly pass through those pixels with lower energies. Fig. 1(d) is the resultant image. Apparently, seam carving keeps well the most important region of interests such as the castle, and does not leave any visually noticeable artifacts such as blurriness. In such a natural manner, seam carving is attractive for content-aware image retargeting.

However, seam carving still might lead to three types of possible artifacts, which include global structure deformation, local texture distortion and information loss [11]. Fig. 2 shows an oversqueezed image by seam carving, in which there is global structural deformation. It is straightforward that objective quality assessment of retargeted image might play an important role in seam carving detection. In the literature, there exist a few approaches for the quality assessment of seam carving. Fang et al. proposed a structural similarity-based objective assessment method for image retargeting [12]. A structural similarity map (SSIM) is defined to indicate how the structural information in source image is preserved in retargeted image. Hsu et al. also presented an objective quality assessment approach for image retargeting by exploiting perceptual geometric distortion and information loss [11]. However, to the best of our knowledge, these existing approaches are full-reference image quality assessment (IQA) approaches [13], which makes them unsuitable for the purpose of blind detection. That is, it is still an open issue to explicitly model retargeting distortions without reference images.

2.2. Most possible clue for seam carving detection

Among the possible artifacts caused by seam carving, geometric distortion is the most annoying since it usually leads to visually unpleasant shape deformation of prominent object. This implies that even without the aid of passive forensics, geometric distortion is highly likely to be perceived by naked eyes. Thus, geometric distortion seldom occurs in practical seam carving detection cases. For information loss, it is also a common concern for seam carving, its quality assessment and blind detection. However, it can be resolved in seam carving by integrating with other resizing techniques such as cropping and adaptive scaling or taking saliency map into the definition of energy function. Actually, seam carving keeps well the main content that an image conveys, especially its semantic information. Unluckily, it is still an unresolved problem to objectively measure the information loss caused by seam carving. Even for full-reference IQA approach, it is not trivial to assess the information loss with the original image as ground truth. In [11], a simple saliency loss ratio (SLR) is presented to measure the information loss. SLR is defined as the percentage of lost saliency map in image retargeting with respect to the original saliency map. Apparently, SLR is image content-dependent, which makes it contribute just a little for IQA. Since original images are unavailable

(a) (b) (c) (d)

Fig. 1. Removing vertical seams: (a) original image; (b) original image with seams marked in red; (c) gradient map with seams marked in red; (d) resultant image after removing 30% seams. (For interpretation of the references to colour in this figure legend, the reader is referred to the web version of this article.)

(a) (b)

Fig. 2. An over-squeezed image by seam carving. (a) original image; (b) resized image with structure deformation.

for the blind detection of seam carving, information loss is not a feasible clue, at least not a good choice at present.

Local texture distortion is the most possible clue for seam carving forgery detection. Firstly, local texture distortion is not as visually unpleasant as geometric deformation, but still brings perceptual impairments to users. Secondly, it makes more sense for the blind forensics of retargeted images without global structure/geometric deformation. This motivates us to address seam carving forgery detection in an analytical and practical way. That is, local texture distortion is further exploited for seam carving detection. Moreover, instead of explicitly modeling local texture distortion, more discriminative texture features are designed by fully considering its perceptual impairments.

3. Brief introduction of LBP and WLD

3.1. LBP

LBP is a simple yet efficient texture descriptor to describe local image pattern. Given a pixel g_c in an image, a pixel-wise LBP code is computed by comparing it with its neighborhood pixels as follows.

$$LBP_{P,R}(x_c, y_c) = \sum_{n=0}^{P-1} \delta(g_n - g_c)2^n \tag{4}$$

where g_c is the central pixel with coordinate (x_c, y_c), and g_n are its neighboring pixels. P is the number of neighboring pixels, and R is the radius of neighborhood. $\delta(\cdot)$ is a sign function. If it meets $g_n \geq g_c$, $\delta(\cdot)$ is given a value of 1, or else 0. Fig. 3 shows the process of basic LBP operator. For an image I of size $N \times M$, let $LBP_{P,R}(i, j)$ be the identified LBP pattern of each pixel (i, j). Then, the image texture is represented by a histogram vector h of length K:

$$H(k) = \sum_{i=0}^{N} \sum_{j=0}^{M} \delta(LBP_{P,R}(i, j), k), \qquad k \in [0, K \tag{5}$$

where $0 \leq k \leq K-1$, and $K = 2^P$ is the number of LBP codes. $\delta(\cdot, \cdot)$ is the Dirac delta function. If $LBP_{P,R}(i, j)$ equals k, then $\delta(\cdot, \cdot)$ equals 1 or else 0. The LBP-based histogram is a widely-used in image analysis applications including texture classification and description.

3.2. WLD

WLD is also a simple yet robust local texture descriptor for digital image [10], which was inspired by Weber's Law. It is composed of two components: differential excitation and orientation. The differential excitation component is to reflect the changes of current pixel. Firstly, the differences between current pixel and its neighbors are computed using the filter f_{00} as follows.

$$x_s = \begin{bmatrix} x_0 & x_1 & x_2 \\ x_7 & x_c & x_3 \\ x_6 & x_5 & x_4 \end{bmatrix}, f_{00} = \begin{bmatrix} +1 & +1 & +1 \\ +1 & -8 & +1 \\ +1 & +1 & +1 \end{bmatrix},$$

$$f_{01} = \begin{bmatrix} 0 & 0 & 0 \\ 0 & +1 & 0 \\ 0 & 0 & 0 \end{bmatrix}, f_{10} = \begin{bmatrix} 0 & -1 & 0 \\ 0 & 0 & 0 \\ 0 & +1 & 0 \end{bmatrix},$$

$$f_{11} = \begin{bmatrix} 0 & 0 & 0 \\ +1 & 0 & -1 \\ 0 & 0 & 0 \end{bmatrix}$$

$$v_s^{00} = \sum_{i=0}^{p-1} (\Delta x_i) = \sum_{i=0}^{p-1} (x_i - x_c) \tag{6}$$

where x_i $(i = 0, 1, \cdots, p-1)$ is the ith neighboring pixel of x_c and p is the number of neighbors. Then, the ratio of the differences to the intensity of current pixel is computed by combining the outputs of two filters f_{00} and f_{01} as follows.

$$G_{ratio}(x_c) = \frac{v_s^{00}}{v_s^{01}} = \sum_{i=0}^{p-1} \left(\frac{x_i - x_c}{x_c} \right) \tag{7}$$

where v_s^{01} is the output of filter f_{01}, which is actually the original image. Finally, the differential excitation $\xi(x_c)$ of current pixel x_c is computed as

$$\xi(x_c) = \arctan(G_{ratio}(x_c)) = \arctan\left(\frac{v_s^{00}}{v_s^{01}}\right) = \arctan\left[\sum_{i=0}^{p-1} \left(\frac{x_i - x_c}{x_c}\right)\right] \tag{8}$$

Let v_s^{11} and v_s^{10} are the outputs of two filters f_{11} and f_{10}, respectively. That is, $v_s^{11} = x_5 - x_1$ and $v_s^{10} = x_7 - x_3$. The gradient orientation component of current pixel is computed as:

$$\theta(x_c) = \arctan\left(\frac{v_s^{11}}{v_s^{10}}\right) \tag{9}$$

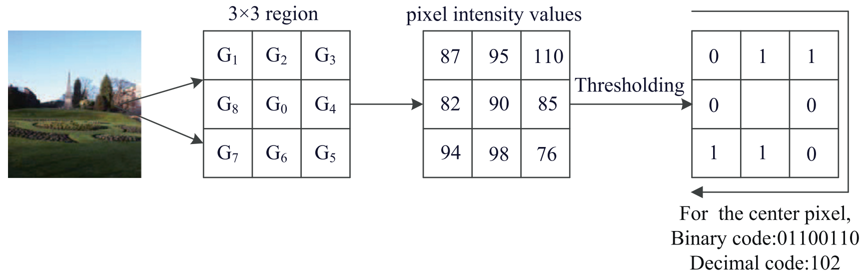

Fig. 3. basic LBP operator.

where θ is within $[-\pi/2, \pi/2]$. Following the values of v_s^{11} and v_s^{10}, θ is mapped to $\theta' \in [0, \pi]$ as follows.

$$\theta'(x_c) = \begin{cases} \theta & v_s^{11} < 0 \quad \text{and} \quad v_s^{10} < 0 \\ \theta + \pi & v_s^{11} > 0 \quad \text{and} \quad v_s^{10} > 0 \\ \theta + \pi & v_s^{11} < 0 \quad \text{and} \quad v_s^{10} > 0 \\ \theta + 2\pi & v_s^{11} > 0 \quad \text{and} \quad v_s^{10} < 0 \end{cases} \tag{10}$$

For simplicity, $\theta'(x_c)$ is further linearly quantized into T dominant orientations as follows.

$$\Phi_t = f_q(\theta') = \frac{2t}{T}\pi \quad \text{and} \quad t = \mathrm{mod}\left(\left\lfloor \frac{\theta'}{2\pi/T} + \frac{1}{2} \right\rfloor, T\right) \tag{11}$$

where T is the number of dominant orientations. If $T = 8$, these dominant orientations are $\Phi_t = (t\pi)/4$, (t=1, 2, …, T-1). After computing each pixel's differential excitation $\xi(x_c)$ using Eq. (8) and orientation Φ_t using Eq. (11), we compute the 2D histogram $WLD(\xi_i, \Phi_t)$, $i = 0, 1, \ldots p-1$, $t = 0, 1, \ldots T-1$. Since the WLD-based histogram is computed pixel-wise, it is a dense descriptor with strong capability of texture description.

4. Proposed method

As claimed in Section 2.2, local texture distortion is the most feasible trace to expose the artifacts left by seam carving. LBP has excellent properties such as low computational cost and strong robustness to illumination variations [14,15]. However, LBP is sensitive to noise and does not provide sufficient information about texture direction. Even different texture patterns might share similar LBP codes in some cases. WLD is a dense descriptor computed for each pixel, which provides stronger texture representation than LBP, especially in capturing local salient patterns. Thus, WLD provides some supplementary texture description with respect to LBP. Inspired by the success of LBP in our earlier approach [8], WLD and LBP are jointly exploited to better reflect the texture variations caused by seam carving. Fig. 4 is the block diagram of the proposed approach. Firstly, color candidate images are transformed into grayscale images. Secondly, the WLD and LBP-based histogram features are extracted from them. Thirdly, Kruskal–Wallis analysis is exploited to select a subset of discriminative features, which are simply fused by concatenation. Finally, SVM is exploited as classifier to decide whether a candidate image is seam-carved or non-seam-carved.

4.1. Extraction of LBP-based and WLD-based histogram features

The dimension of LBP-based features depends on the selection of R and corresponding P. In this paper, we select $R = 1$ and $P = 8$ (since LBP is computed in a 3×3 neighborhood) by experiments. That is, only 8-connected neighboring pixels are involved in computing LBP. By recursively computing the LBP value for each pixel, the input image is transformed into LBP domain. Thus, the LBP(8,1) operator produces a 256D histogram feature.

For the WLD-based histogram $\{WLD(\xi_j, \theta_t)\}$, (j=0, 1,…, N-1, t=0, 1, …, T-1), it is computed from both differential excitation $\xi(x_c)$ and orientation θ. N is the dimensionality of an image, and T is the number of dominant orientations. Thus, the dimension of this histogram is $T \times C$, where C is the number of cells in each orientation. That is, each column corresponds to a direction θ and each row corresponds to a differential excitation histogram with S bins. The WLD-based histogram is computed for each block. Fig. 5 shows the procedure of WLD histogram $\{WLD(\xi_j, \theta_t)\}$. Let M be the number of segments of each sub-histogram. In this paper, an image is divided into 3×3 blocks, and θ is divided into 8 orientations (from $-\pi/2$ to $\pi/2$) for each block. Moreover, an 8D histogram is extracted from each orientation. That is, the selected parameters are T=3, M=8, S=8. Finally, the whole image is considered as a block to obtain the 64D histogram features from 8 orientations. Thus, the dimension of the WLD-based histogram features is 640, which equals to $[(3 \times 3)+1] \times 8 \times 8$.

Though WLD also computes the difference between center pixel and its neighbors as LBP, the differences are summed and then divided by the value of center pixel to obtain the differential excitation. Moreover, WLD has extra gradient orientation to describe texture directions. Thus, WLD provides stronger texture descriptions, which motivates us to exploit both WLD-based and LBP-based histogram features. To prove the effectiveness of the LBP-based and WLD-based histogram features, a preliminary experiment is conducted to show their changes when an original image is removed 10%, 20% and 30% seams, respectively. Fig. 6 reports the experimental results. Fig. 6(a) is the original image, Figs. 6(b)–(d) are the images with 10%, 20% and 30% seams to be removed, respectively. Figs. 6(e) and (f) are the LBP-based and WLD-based histograms for the original image and the resized images. From Figs. 6(e) and (f), we can observe that with the increment of scaling ratios, there are trends of local peak descending for both LBP-based and WLD-based histograms.

4.2. Kruskal–Wallis test for feature selection

The LBP-based and WLD-based histogram features are 256D and 640D, respectively. Thus, we obtain 896D features. Since some features may contribute little to detection accuracy but bring computational complexity, feature selection is used to remove irrelevant and/or redundant features. In this paper, Kruskal–Wallis test is selected for feature selection due to its simplicity [16,17]. The Kruskal–Wallis method is a non-parametric, one-way ANOVA (i.e., analysis of variance) test. It tests the hypothesis whether the samples from two or more groups have equal medians, and returns a value p. If p is close to zero for some specific feature, this feature is selected as it is expected to have good discriminative power. For the details about the Kruskal–Wallis test, please refer to [17]. Here,

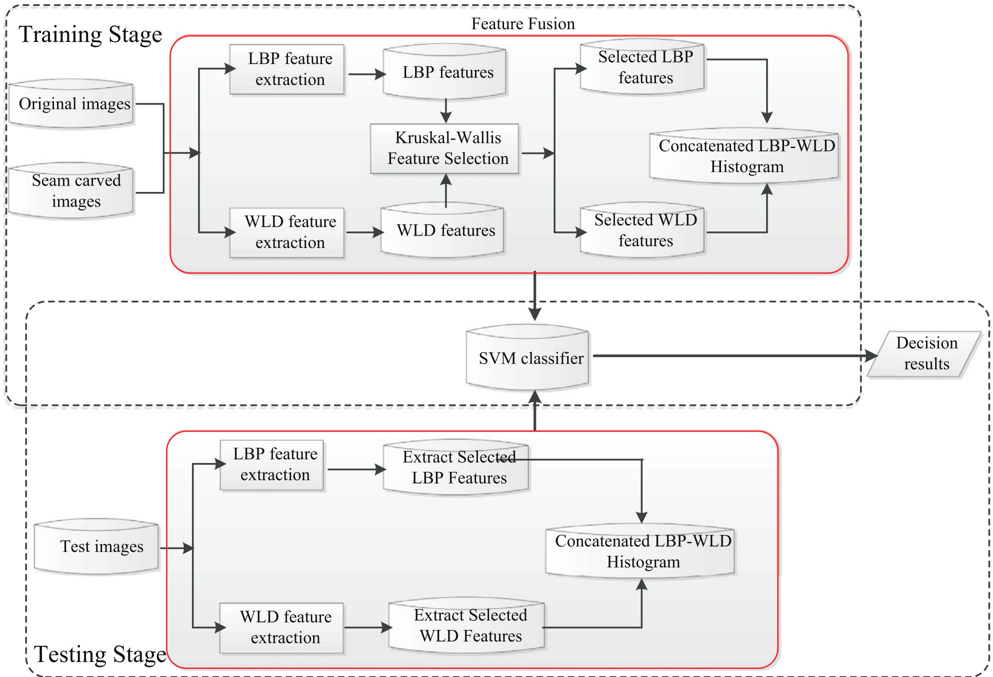

Fig. 4. Block diagram of the proposed approach.

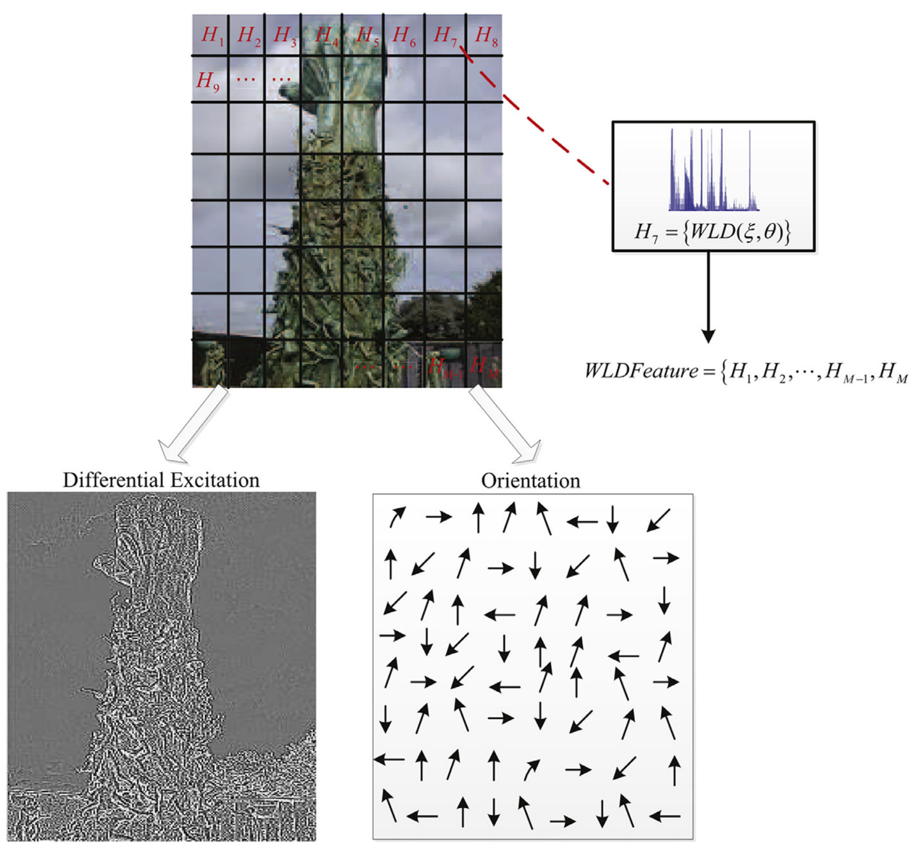

Fig. 5. The extration and representation of WLD features.

the Kruskal–Wallis method is adopted to select the LBP-based and WLD-based histogram features, respectively. Those features that have p values less than a threshold are selected, and their indices are stored. During the testing stage, only those selected features are used for final classification.

4.3. SVM For blind forensics

Blind forensics is actually a binary classification problem. Thus, some conventional classifiers widely used in pattern classification are also exploited for image forensics. It is well-known that SVM is a supervised learning model for binary linear classifier [18], which

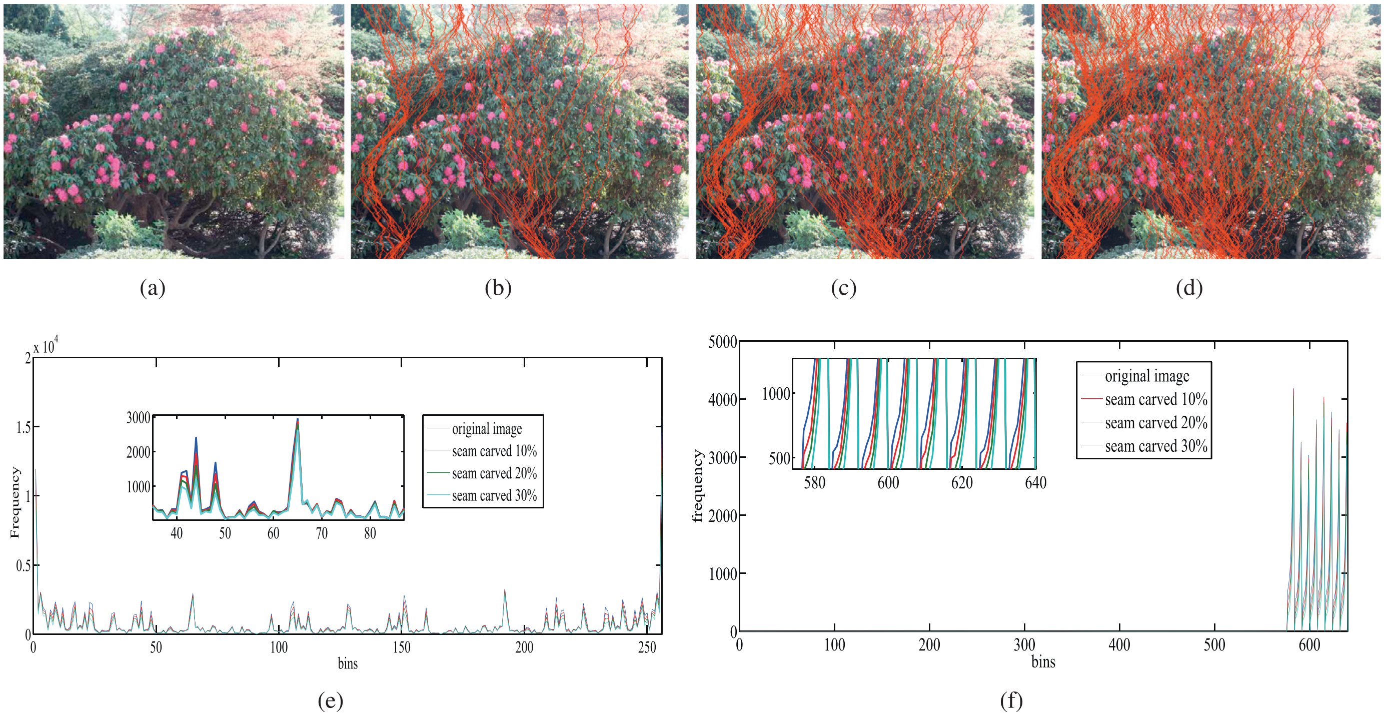

Fig. 6. The changes of the WLD and LBP histogram features before and after seam carving: (a) original image; (b) original image with 10% seams; (c) original image with 20% seams; (d)original image with 30% seams;(e) the LBP histogram;(f) the WLD histogram.

is based on the concept of decision planes that define decision boundaries. In this paper, SVM is also adopted as classifier for its simplicity to train and test the feature sets, which are extracted from candidate images. Radial Basis Function (RBF) is adopted as the kernel function to non-linearly project the extracted feature vectors into a high dimensional feature space. In the training stage, two classes of images (seam-carved or not-carved) are described by both selected WLD histogram and LBP histogram features. Then, SVM attempts to find an optimal linear decision surface called the maximum margin hyper plane by maximizing the geometric margin between the closest instances on either side. In the final classification stage, the feature vectors extracted from candidate images are input into SVM for binary classification. That is, each candidate image will be classified into either class of seam-carved image or non-carved image.

5. Experimental results and analysis

5.1. Experiment setup

To test the proposed approach, experiments are conducted with a personal computer (Intel Core i3-2400 CUP @3.4GHz, 4GB Memory, Windows XP) and the detector is implemented with Matlab2010a. To the best of our knowledge, there is still no public-available image database of seam carving, which can be directly used for seam carving forgery detection. Thus, we build an image dataset for seam carving detection by ourselves. Firstly, Uncompressed Colour Image Database (UCID) [19], which is widely used for IQA, is chosen as the benchmark dataset. There are 1338 color images in UCID v2 database. These images have rich contents including landscape, building, flowers, human, animals, and so on. Then, these images are resized by the original seam carving method [2] with multiple scaling ratios. The resized images are divided into three groups in the experiment. (1) images with small scaling ratios; (2) images with large scaling ratios; and (3) images with mixed scaling ratios. In the first case, the scaling ratios vary from 3% to 21% with a step size of 3%. That is, the scaling ratios are 3%, 6%, 9%, 12%, 15%, 18% and 21%, respectively. Thus, there are totally 1338 original images and $1338 \times 7 = 9366$ seam carved images. In the second case, the scaling ratios vary from 10% to 60% with a step size of 10%. Thus, there are $1338 \times 6 = 8028$ tampered images. In the third case, the tampered images for the above two cases are mixed to form a new image database for test. Thus, there are 1338 original images and $9366 + 8028 = 17394$ tampered images. To make sufficient comparisons, three state-of-the-art approaches including Wei et al. [6], Ryu et al. [7] and Yin et al. [8] are chosen as benchmarks for performance evaluation. That is, there are totally four detectors including the proposed approach, which are tested in the same experimental environments including hardware, software and test image database. SVM is directly downloaded from [20], and the Radial Basis Function(RBF) is used as the basic kernel function. To obtain the optimal parameters of kernel function, a grid-search technique is exploited by a 5-fold cross-validation strategy. Moreover, Python and Gnuplot are used for parameter optimization.

Table 1
Number of features selected using different p values.

P value	0.001	0.003	0.005	0.007	0.009	Full
number of LBP features	27	58	106	155	204	256
number of WLD features	153	245	352	446	515	640

5.2. Feature selection

The Kruskal–Wallis test is exploited to select discriminative features from the LBP-based and WLD-based histogram features. To find an optimum threshold for discarding redundant histogram features, the value of p (significance) varies within [0.001 0.01] with an increment of 0.002. Table 1 shows the number of selected LBP and WLD features with different p values. Fig. 7 shows the detection accuracies for scaling ratios of 3%, 6%, 9% and 12% by se-

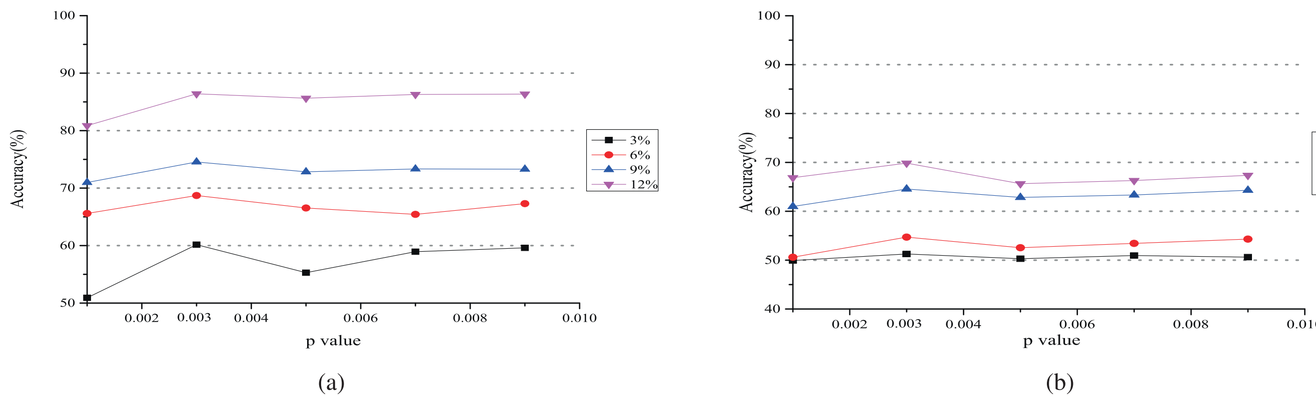

Fig. 7. Effect of Krukal–Wallis technique: (a) Effect of Krukal–Wallis technique with LBP; (b) Effect of Krukal–Wallis technique with WLD.

Table 2
Comparisons of detection accuracy for carved images with small scaling ratios.

Scaling ratio(%)	Accuracy(%)			
	Wei et al. [6]	Ryu et al. [7]	Yin et al. [8]	Our approach
3	50.22	54.48	55.53	68.26
6	53.59	57.88	65.17	84.99
9	56.99	60.99	74.55	89.86
12	58.21	64.13	81.20	92.72
15	63.13	70.59	90.17	95.03
18	71.94	73.84	92.04	95.94
21	74.78	76.91	94.32	96.02

Table 3
Comparisons among four detectors for the mixed dataset with small scaling ratios.

Scaling ratio(%)	Accuracy(%)			
	Wei et al. [6]	Ryu et al. [7]	Yin et al. [8]	Our approach
3	22.32	34.18	29.29	31.32
6	27.24	40.89	39.32	50.84
9	34.14	45.16	51.77	69.86
12	38.54	50.48	62.16	85.29
15	47.59	58.06	87.01	92.65
18	52.91	61.90	93.11	94.37
21	56.64	67.31	97.21	97.38

lecting features with six representative p values. It is apparent that the best detection accuracy is achieved with a p value of 0.03. Under this case, the LBP-based and WLD-based histogram features are 58D and 245D, respectively. In the following, experimental results are reported with the selected histogram features in the case of p=0.003.

5.3. Experimental results of seam carved images with different scaling ratios

For each scaling ratio, there are 1338 original images and 1338 retargeted images. To ensure the randomness of our experiments, they are equally divided into five shares of the same number of samples. For each round of training and testing, four shares are randomly chosen as a testing set and the rest share is used as a training set. The training and testing are repeated for five times and the average results are reported.

5.3.1. Images with small scaling ratios

Those seam carved images with small scaling ratios are firstly tested to evaluate the performance of the proposed approach. Table 2 compares the detection accuracies among four detectors. We can observe that the detection accuracies also increase with the increment of scaling ratio, and the proposed approach achieves the best detection accuracies among them. For the patch-based approach [6], it only considers the optimal type of patches for each mini-square. Thus, it does not explicitly consider the changes of local texture caused by image seam carving. The detector by Ryu et al. [7] exploits the energy bias and noise level of an image to expose seam carving forgery. Compared with the patch-based detector [6], the energy bias-based approach [7] is more closely related with the inherent nature of seam carving. Therefore, its detection accuracy is superior to the patch-based approach [6]. The LBP-based detector [8] extracts the energy bias, noise and half seam-based features in LBP domain, instead of the conventional pixel-domain. It is actually an improvement to the energy-based approach [7] by extracting features in LBP domain. For this season, the LBP-based detector [8] achieves superior detection accuracy over the patch-based detector [6] and the energy bias-based approach [7], respectively. For the proposed approach, it simultaneously exploits two complimentary texture descriptors WLD and LBP to expose local texture changes. Thus, it is the most effective to expose seam carving with small scaling ratios.

Moreover, the mixed image set with small scaling ratios is further experimented. Firstly, we randomly select 268 images from the 1338 seam carved images for each scaling ratio. Thus, there are totally $268 \times 7 = 1876$ forgery images, which are merged with the 1338 original images to form a mixed set with 3214 images for training. The rest 7490 resized images are used as the dataset for

Table 4
Comparison of detection accuracy for carved image with large scaling ratios.

Scaling ratio(%)	Accuracy(%)			
	Wei et al. [6]	Ryu et al. [7]	Yin et al. [8]	Our approach
10	57.91	65.22	80	93.05
20	74.18	75.37	94.48	95.99
30	91.34	85.52	98.66	97.58
40	89.70	91.94	99.85	98.64
50	94.93	96.27	99.85	99.20

Table 5
detection accuracy of mixed sets with large scaling ratios.

Scaling ratio(%)	Accuracy(%)			
	Wei et al. [6]	Ryu et al. [7]	Yin et al. [8]	Our approach
10	24.67	32.80	51.78	54.88
20	61.59	61.68	93.55	97.53
30	89.35	83.46	99.35	98.42
40	91.03	95.23	99.81	98.82
50	95.89	98.78	100	98.97

Table 6
The F_1 score comparison for the seam carved images on the different scaling ratios.

Scaling ratio(%)	F_1 score(%)			
	Wei et al. [6]	Ryu et al. [7]	Yin et al. [8]	Our approach
3	50.12	59.97	57.52	67.10
6	60.60	61.42	69.27	80.93
9	61.54	62.49	79.91	89.82
12	64.46	67.13	84.83	90.92
15	96.98	73.07	95.23	96.73
18	92.82	75.33	97.10	97.81
21	83.02	79.07	97.97	98.31
30	98.54	88.48	99.14	98.52
40	96.00	95.91	99.81	99.32
50	98.29	97.87	99.88	99.62

Table 7
Results with and without fusion.

Scaling ratio(%)	Accuracy(%)				
	WLD	WLD+feature selection	LBP	LBP+feature selection	final LBP and WLD features
3	51.34	51.26	60.43	60.16	68.26
6	54.26	54.71	69.84	69.71	84.99
9	63.15	64.55	74.91	74.55	89.86
12	69.91	69.84	87.18	87.4	92.72
15	79.11	79.25	91.94	92.10	95.03
18	83.10	83.33	93.24	93.54	95.94
21	85.16	85.36	95.50	95.65	96.02
30	90.88	91.20	96.43	96.63	97.58
40	92.89	93.10	97.70	97.88	98.64
50	95.22	95.89	98.77	98.98	99.20

Table 8
comparisons of time consumption among four detectors.

Detection method	Computation time
Wei et al. [6]	8.1123
Ryu et al. [7]	0.7825
Yin et al. [8]	0.6497
Proposed approach	1.9881

performance evaluation. From the experimental results reported in Table 3, the proposed approach also achieves the best detection performance.

5.3.2. Images with large scaling ratios

Table 4 reports the experimental results for resized images with large scaling ratios including 10%, 20%, 30%, 40% and 50%, respectively. For those images with scaling ratios of 10% and 20%, the proposed approach achieves the best detection accuracies among four detectors. Moreover, the detection accuracies are more than 90% for the resized images with each scaling ratio. When the scaling ratios are over 30%, the detection accuracies of the proposed approach are slightly worse than the LBP-based approach [8]. Please note that as claimed in the introduction section, when an image is resized with large scaling ratio up to 30%, there are usually visually annoying structure deformation. Under this case, it is not difficult for users to judge seam carving forgery, even without the aid of passive forensics.

To further explain the detection performance of the proposed approach, the mixed set of resized images with large scaling ra-

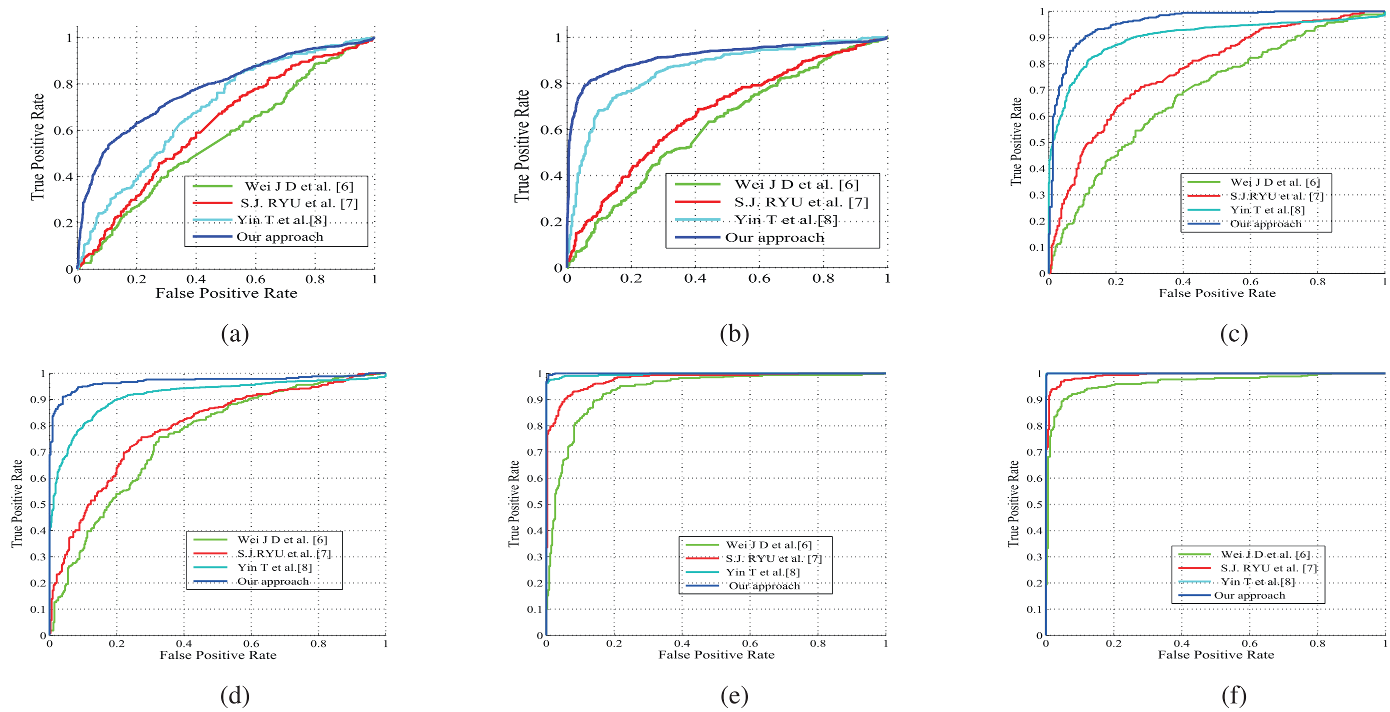

Fig. 8. Comparison of ROC curves among four detectors,(a) scaling ratio of 6%; (b) scaling ratio of 10%; (c) scaling ratio of 15%; (d) scaling ratio of 20%; (e) scaling ratio of 30%; (f) scaling ratio of 50%.

tios is also experimented. Table 5 reports the experimental results. When the scaling ratios are no more than 20%, the proposed approach also achieves the best detection accuracy among four detectors. For the scaling ratios are more than 30%, the detection accuracy of the proposed approach is only slightly lower than Yin et al. [8].

5.3.3. *Images with mixed scaling ratios*

To verify the robustness of the proposed method, those retargeted images with large and small scaling ratios are mixed together for further experiments. Fig. 8 shows the ROC curves of four detectors, in which each sub-figure represents the ROC performance under different scaling ratios from 6% to 50%, respectively. When the scaling ratio exceeds 10%, the proposed approach achieves the best performances among four detectors. Moreover, the proposed approach has steadier ROC curves than the rest three detectors when the scaling ratios are over 20%.

5.4. *The* F_1 *score on the different scaling ratios*

In statistical analysis of binary classification, F1 score is a widely-accepted measure for classification accuracy [21]. To further prove the effectiveness of the proposed approach, we compare the F_1 score (also known as F-score or F-measure) among the four detectors. The definition of the F_1 score is as follows.

$$F_1 = \frac{(\gamma^2 + 1) \cdot Precision \times Recall}{\gamma^2 \cdot Precision + Recall} \tag{12}$$

where

$$Precision = \frac{TP}{TP + FP}, \qquad Recall = \frac{TP}{TP + FN}$$

In Eq. (12), γ controls the balance between *Precision* and *Recall*, and γ is normally set to 1. Thus, the F1 score can be interpreted as a weighted average of *Precision* and *Recall*. The higher the F-score is, the better the classification is. An F1 score reaches its best value at 1 and worst at 0. *TP*, *FP* and *FN* are true positive, false positive and false negative samples, respectively. In this paper, the original images and the seam carved images are denoted as positive samples and negative samples, respectively. Table 6 summarizes the result of F_1 score comparisons among four detectors. From it, the proposed approach achieves higher F_1 scores than three existing methods for those seam carved images with small scaling ratios. For seam carved images with scaling ratios above 30%, Yin et al. [8] achieves slightly higher F_1 scores than the proposed approach.

5.5. *Other analysis*

Table 7 compares the detection accuracies by LBP features, WLD features and both. It also compares with the detection accuracies before and after feature selection with the Kruskal–Wallis test. From it, the combined LBP-based and WLD-based histogram features achieves better accuracies than the LBP-based features or the WLD-based features alone. This proves that the WLD-based features provide complementary information to the LBP-based features, which improves the accuracies. Moreover, the Kruskal–Wallis test is effective for feature selection for the proposed approach,simply because there are no signification decreases of detection accuracy after it.

Computational complexities are also compared among the proposed approach and three existing works. Because four detectors are running under the same experimental environment, the comparison of computational complexity is directly made by their actual time consumptions. Because four detectors share similar classification mechanism, Table 8 only reports the actual time consumptions of feature extraction. From Table 8, the proposed approach consumes much less time than the patch-based approach [6], but consumes more time than the energy-based approach [7] and the single LBP-based approach [8]. Please note that the computational complexity of the proposed approach is still within an acceptable range for practical forensics.

6. Conclusion

Seam carving is a popular content-aware image resizing technique. However, it can also produce faked images without degradation of perceptual quality. From the qualitative analysis of possible artifacts caused by seam carving, we infer that local texture distortion is the most possible clue for its forgery detection. Instead of explicitly modeling local texture distortion, we design some measurable features to expose the texture change caused by seam carving. Specifically, we present a blind seam carving detection approach by exploiting both the WLD-based and LBP-based histogram features. The Kruskal–Wallis test is exploited to select an optimal feature subset from them. The experimental results show that the proposed approach achieves better detection accuracies than the state-of-the-art approaches. For future work, we will attempt to exploit information loss and global geometric distortion for seam carving forgery detection. Further, since there are a few image resizing techniques besides seam carving, we will also attempt to identify the adopted image resizing technique for resized images. Since this is a multi-classification problem rather than binary decision, more discriminative features should be designed from other points of view [22–24] and stronger classifiers such as incremental support vector learning [25–27] can be considered.

Acknowledgments

This work is supported in part by the National Natural Science Foundation of China (61572183, 61379143, 61232016, 61672222, 61772087), the Scientific Research Fund of Hunan Provincial Education Department of China (14C0029).

References

[1] Piva A. An overview on image forensics. ISRN Signal Process 2013:1–23.
[2] Avidan S, Shamir A. Seam carving for content-aware resizing. ACM Trans Graph 2011;26(3):10–16.
[3] Lu W, Wu M. Seam carving estimation using forensic hash. In: Proceedings of the thirteenth ACM multimedia workshop on multimedia and security. ACM; 2011. p. 9–14.
[4] Sarkar A., Nataraj L., Manjunath B.S.. Detection of seam carving and localization of seam insertions in digital images. Proceedings of the 11th ACM workshop on multimedia and security. ACM; 2009, 107–116.
[5] Fillion C, Sharma G. Detecting content adaptive scaling of images for forensic applications. SPIE electronic imaging, International Society for Optics and Photonics 2010;75410Z:112.
[6] Wei JD, Lin YJ, Wu YJ. A patch analysis method to detect seam carved images. Pattern Recognit Lett 2014;36:100–6.
[7] Ryu SJ, Lee HY, Lee HK. Detecting trace of seam carving for forensic analysis. IEICE Trans Inf Syst 2014;97(5):1304–11.
[8] Yin T, Yang G, Li L, et al. Detecting seam carving based image resizing using local binary patterns. Comput Secur 2015;55:130–41.
[9] Hong X, Zhao G, Pietikainen M, et al. Combining LBP difference and feature correlation for texture description. IEEE Trans Image Process 2014;23(6):2557–68.
[10] Chen J, Shan S, He C, et al. WLD: a robust local image descriptor. IEEE Trans Pattern Anal Mach Intell 2010;32(9):1705–20.
[11] Hsu CC, Lin CW, Fang Y, et al. Objective quality assessment for image retargeting based on perceptual geometric distortion and information loss. IEEE J. Sel. Top. Signal Process. 2014;8(3):377–89.
[12] Fang Y, Zeng K, Wang Z, et al. Objective quality assessment for image retargeting based on structural similarity. IEEE J. Emerging Sel. Top. Circuits Syst. 2014;4(1):95–105.
[13] Ma L, Lin W, Deng C, et al. Image retargeting quality assessment: a study of subjective scores and objective metrics. IEEE J. Sel. Top. Signal Process. 2012;6(6):626–39.
[14] Muhammad G, Hussain M, Alenezy F, et al. Race classification from face images using local descriptors. Int. J. Artif. Intell. Tools 2012;21(5):1250019.
[15] Ullah I, Aboalsamh H, Hussain M, et al. Gender classification from facial images using texture descriptors. J. Internet Technol. 2014;15(5):801–12.
[16] Huan L, Hiroshi M, Rudy S, et al. Feature selection: an ever evolving frontier in data mining. In: The fourth workshop on feature selection in Data Mining(FSDM10); 2010. p. 4–13.
[17] Yvan S, Inaki I, Pedro L. A review of feature selection techniques in bioinformatics. Bioinformatics 2007;23(19):2507–17.
[18] Chang CC, Lin CJ. LIBSVM: a library for support vector machines. ACM Trans Intell Syst Technol 2011;2(3):27–32.
[19] Schaefer G, Stich M. UCID: an uncompressed color image database. International Society for Optics and Photonics; 2003. p. 472–80.
[20] LIBSVM: a library for support vector machine. http://www.csie.ntu.edu.tw/~cjlin/libsvm/.
[21] Li J, Li X, Yang B, et al. Segmentation-based image copy-move forgery detection scheme. IEEE Trans Inf Forensics Secur 2015;10(3):507–18.
[22] Zhou ZL, Wang YL, Wu QM, et al. Effective and efficient global context verification for image copy detection. IEEE Trans Inf Forensics Secur 2017;12(1):48–63.
[23] Zhou ZL, Yang CN, Chen BJ, et al. Effective and efficient image copy detection with resistance to arbitrary rotation. IEICE Trans Inf Syst 2016;E99-D(6):1531–40.
[24] Wang J., Li T., Shi Y.Q., et al. Forensics feature analysis in quaternion wavelet domain for distinguishing photographic images and computer graphics. Multimed Tools Appl 2016; DOI:10.1007/s11042-016-4153-0.
[25] Gu B, Sun XM, Sheng VS. Structural minimax probability machine. IEEE Trans Neural Netw Learn Syst 2016;28(7):1646–56.
[26] Gu B, Sheng VS. A robust regularization path algorithm for ν-support vector classification. IEEE Trans Neural Netw Learn Syst 2017;28(5):1241–8.
[27] Gu B, Sheng VS, Tay KY, et al. Incremental support vector learning for ordinal regression. IEEE Trans Neural Netw Learn Syst 2015;26(7):1403–16.